CHAPTER – 2

ONE-DIMENSIONAL PHOTONIC CRYSTAL COMPOSED OF LINEAR GRADED MATERIALS

2.1 Introduction

Photonic band gap (PBG) property of the photonic crystals (PCs) can be used to confine, manipulate and control photons, and leading to a key role for all integrated optical devices technology [Lipson (2009)]. Over the past several years, one-dimensional (1-D) PCs have been intensively investigated with different materials such as dielectric, anisotropic, negative refractive index, magnetic materials etc. [Tolmachev (2008); Negro (2005); Alagappan (2006); Zharov (2008); Vasconcelos (2007); Yu (2007)]. 1-D PCs have many potential applications in optical communication and optoelectronics such as reflecting mirrors, waveguides, optical switches, filters, detectors, light emitting diode, etc. Moreover, one of the very interesting properties of the PCs is omnidirectional band gap (OBG) by which light in a particular frequency region from the entire incident angle is totally reflected in both transverse electric (TE) and transverse magnetic (TM) polarization. The absolute OBGs have been demonstrated theoretically and experimentally in 1-D PCs [Fink (1998); Yablonovitch (1998); Seeser (1999); Xiang (2010)]. OBG properties can potentially be used to improve the performance of reflectors, filters, detectors, and optical fibers, etc.

Recently, several researchers have proposed 1-D PCs with the gradual variation of refractive index or width of layers in the direction perpendicular to the surface of layers [Rauh (2010); Sang (2006); Pandey (2008)]. Such structures are called graded photonic crystals (GPCs). Gradual variation of the relative parameters in GPCs makes them very different from the conventional PCs in terms of enhancing the performance to confine, manipulate and guide light wave propagation [Centeno (2005); Kurt (2007); Ren (2011)]. Such types of PCs play an important role in designing spectral filters, high efficiency bending waveguides, couplers, self-focusing media and antireflection coating etc. [Wang (2011); Oner (2013); Cakmak (2009); Vasic (2011); Chhajed (2008)].

Motivated by the ability to manipulate, confine and control of the light by different types of GPCs. Herein, the study of the tunability of photonic and Omni-

directional band gaps and defect mode properties in 1-D PCs constituted with linear graded index materials has been presented. The refractive index of the graded materials layer varies in a linear fashion as a function of the depth of graded layer. We have first provided the theoretical models and calculation of the reflectance, transmittance and band structure of 1-D PC structures with linear graded index materials. Next, the influences of linear graded index layers on the photonic and omnidirectional band gap and defect modes properties in 1-D PC structures have been investigated. In this Section, the study has been carried out as follows. First, the reflection spectra and band structure for different layer thicknesses and various refractive index of the constituted normal layer have presented. Second, the properties of OBG for the structures with quarter-wave and latent type layer stacking arrangements have investigated. Third, the effects of the grading parameters on the PBG in 1-D GPC structures have studied. Next, transmission spectra and defect modes for the 1-D PC structures with a defect layer of linear graded index material at different periodicity, defect layer thickness and grading parameter have also demonstrated. Moreover, the effect of incident angle on the defect modes for transverse-electric (TE) and transverse-magnetic (TM) polarizations have also investigated. Finally, the results are briefly summarized.

2.2 Theoretical description

Considered 1-D GPC structures are composed of two types of dielectric layers. One is the graded layer (A or A′) with linear variation of refractive index as a function of layer thickness and the other is homogeneous layer (B) with space independent refractive index. The schematic views of 1-D GPC structures (Type1 and Type2) are shown in figure 2.1. Type1 is the periodic structure of like $(AB)^N$ and Type2 is the periodic structure of like $(A'B)^N$, where N represents the number of periods. The widths of the graded and homogeneous layers are d_1 and d_2, respectively. Refractive index distributions in the graded layer A and A′ vary in two different ways with layer thickness. For layers A, the index of refraction increases linearly from initial ($x = 0$) to the end ($x = d_1$) boundaries of the graded layer, which is expressed as:

$$\left[\boldsymbol{n(x) = n_i + \frac{(n_f - n_i)}{d_1} \times x}\right] \quad \text{… …} \quad \textbf{(2.1)}$$

However, the variation of refractive index decreases linearly from initial to the end boundaries of graded layers A′, which is expressed as:

$$\left[n(x) = n_f + \frac{(n_i - n_f)}{d_1} \times x\right] \quad \ldots\ldots \quad (2.2)$$

where n_i and n_f are lower and higher index of refraction in the graded layers respectively, and d_1 is the layer thickness. Subscript i and f represent the lower and higher refractive index positions in graded layers, respectively.

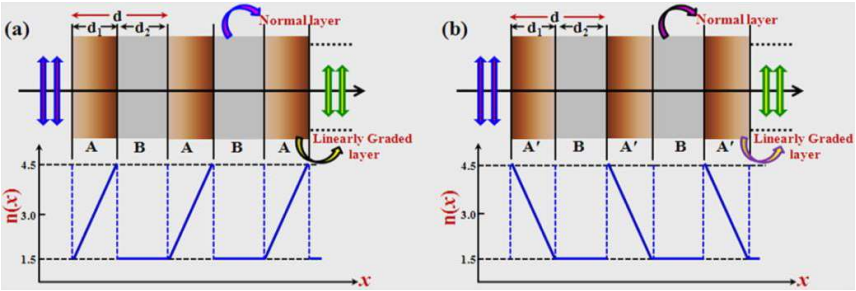

Figure 2.1 Schematic representation of one-dimensional graded photonic crystal structures with linearly (a) increasing and (b) decreasing refractive index in a linear graded layer.

The electric field distribution for light wave propagation in a graded layer with linearly increasing refractive index along perpendicular to the surface of graded layer is given by [Yeh (1988)];

$$E_G(x) = \sqrt{\xi}\,.\left[A_L J_{\frac{1}{4}}\left(\frac{\xi^2}{2\alpha}\right) + B_L Y_{\frac{1}{4}}\left(\frac{\xi^2}{2\alpha}\right)\right] \quad \ldots\ldots \quad (2.3)$$

where A_L and B_L are constants for the linear graded layers, and $\xi = \omega.n(x).cos\theta_L/c$ is the propagation wave vector for an angle of incidence θ_L and the angular frequency ω, and c is the speed of light. Refractive index $n(x)$ is taken according to linearly increasing or decreasing refractive index in a linear graded layer (A or A') as defined by the equations (2.1) and (2.2), respectively. $J_{1/4}$ and $Y_{1/4}$ are $(1/4)^{th}$- order of first and second kinds Bessel functions, respectively. Subscript L represents graded layer. $\alpha = (\omega/c).\left((n_f - n_i)/d_1\right)$ is the grading profile parameter. For the linear graded layer with linearly decreasing refractive index, the electric field distribution is in the same form except α which is replaced by α', where $\alpha' = (\omega/c).\left((n_i - n_f)/d_1\right)$.

The electric field distribution for a homogeneous layer along x-axis is given by;

$$E_H(x) = A_H\, exp(-ik_H x) + B_H\, exp(ik_H x) \quad \ldots\ldots \quad (2.4)$$

where A_H and B_H are constants, k_H is the wave vector and subscript H represents a homogeneous layer.

Multilayer interface optics can be generally described as the use of the amplitudes and phases of light reflected (or transmitted) at material boundaries to produce

interference effects. To attain the reflectance (R) and transmittance (T), it is necessary to calculate the reflection and transmission coefficients of the fields in the incident and outgoing media, labeled as r and t, respectively. Because partially transmitted and reflected waves are generated at each interface present in the multilayer, the expression for the electric field, which is perpendicular to the plane of incidence, in each one of the slabs in the periodic structure $(AB)^N$ can be expressed as;

$$E(x) = \begin{cases} A_0\, e^{-ik_0 x} + B_0\, e^{ik_0 x}, & x \le x_0 \\ \sqrt{\xi}_{(x-x_0)} \left[A_1 J_{\frac{1}{4}}\left(\frac{\xi^2}{2\alpha}\right)_{(x-x_0)} + B_1 Y_{\frac{1}{4}}\left(\frac{\xi^2}{2\alpha}\right)_{(x-x_0)} \right], & x_0 \le x \le x_1 \\ A_2\, e^{-ik_H(x-x_1)} + B_2\, e^{ik_H(x-x_1)}, & x_1 \le x \le x_2 \\ \sqrt{\xi}_{(x-x_2)} \left[A_3 J_{\frac{1}{4}}\left(\frac{\xi^2}{2\alpha}\right)_{(x-x_2)} + B_3 Y_{\frac{1}{4}}\left(\frac{\xi^2}{2\alpha}\right)_{(x-x_2)} \right], & x_2 \le x \le x_3 \\ \cdots\cdots\cdots & \cdots\cdots\cdots \\ \cdots\cdots\cdots & \cdots\cdots\cdots \\ \cdots\cdots\cdots & \\ A_{2n}\, e^{-ik_H(x-x_{2n-1})} + B_{2n}\, e^{ik_H(x-x_{2n-1})}, & x_{2n-1} \le x \le x_{2n} \\ A_{2n+1}\, e^{-ik_0(x-x_{2n})}, & x_{2n} \le x \end{cases} \quad \cdots\cdots \quad (2.5)$$

with

$$\begin{gathered} x_0 = 0, \\ x_1 = d_1, \\ x_2 = x_1 + d_2 = d_1 + d_2 = d, \\ x_3 = x_2 + x_1 = d_1 + d_2 + d_1 = d + d_1, \\ \cdots\cdots\cdots \\ x_{2n-1} = (N-1)d + d_1, \\ x_{2n} = Nd, \\ N = 2n. \end{gathered}$$

where k_0, k_H and ξ are the wave vectors in the air, homogeneous and graded media, respectively, n represents the n^{th} media and N is the number of periods. In the considered media, the electric field is taken to be the sum of a propagating and a counter-propagating wave with similar wave vectors but opposite direction and amplitude which given by the coefficients labelled generally as A_j and B_j (j = 0, 1, 2 …), respectively. Similarly, the expression of electric field in each one of the slabs in the periodic structure $(A'B)^N$ can be written as above equation, only propagation wave vector (ξ) and grading profile parameter changes according to layers A'.

In case of TE-polarization, all electric field vectors are perpendicular to the plane of incidence, and the magnetic field vectors are chosen to give a positive energy flow in the direction of the wave vectors. The frequency dependent coefficients A_j and B_j are determined by imposing continuity conditions for both the electric field and magnetic field across the interface from one medium to the next. This establishes a set of

equations that we solve by making use of the transfer matrix formalism. Under this formalism, the set of equations can be expressed as;

$$\underbrace{\begin{pmatrix} 1 & 1 \\ ik_0 & -ik_0 \end{pmatrix}}_{M_0}\begin{pmatrix} A_0 \\ B_0 \end{pmatrix}$$

$$= \underbrace{\begin{pmatrix} \sqrt{\xi_0}.J_{\frac{1}{4}}\left(\frac{\xi_0}{2\alpha}\right) & \sqrt{\xi_0}.Y_{\frac{1}{4}}\left(\frac{\xi_0}{2\alpha}\right) \\ -\xi_0\left(\frac{\alpha}{2\xi_0^{3/2}}.J_{\frac{1}{4}}\left(\frac{\xi_0}{2\alpha}\right)+\xi_0^{1/2}.J_{\frac{1}{4}}'\left(\frac{\xi_0}{2\alpha}\right)\right) & -\xi_0\left(\frac{\alpha}{2\xi_0^{3/2}}.Y_{\frac{1}{4}}\left(\frac{\xi_0}{2\alpha}\right)+\xi_0^{1/2}.Y_{\frac{1}{4}}'\left(\frac{\xi_0}{2\alpha}\right)\right) \end{pmatrix}}_{M_i}\begin{pmatrix} A_1 \\ B_1 \end{pmatrix}$$

$$\underbrace{\begin{pmatrix} \sqrt{\xi_1}.J_{\frac{1}{4}}\left(\frac{\xi_1}{2\alpha}\right) & \sqrt{\xi_1}.Y_{\frac{1}{4}}\left(\frac{\xi_1}{2\alpha}\right) \\ -\xi_1\left(\frac{\alpha}{2\xi_1^{3/2}}.J_{\frac{1}{4}}\left(\frac{\xi_1}{2\alpha}\right)+\xi_1^{1/2}.J_{\frac{1}{4}}'\left(\frac{\xi_1}{2\alpha}\right)\right) & -\xi_1\left(\frac{\alpha}{2\xi_1^{3/2}}.Y_{\frac{1}{4}}\left(\frac{\xi_1}{2\alpha}\right)+\xi_1^{1/2}.Y_{\frac{1}{4}}'\left(\frac{\xi_1}{2\alpha}\right)\right) \end{pmatrix}}_{M_f}\begin{pmatrix} A_1 \\ B_1 \end{pmatrix}$$

$$= \underbrace{\begin{pmatrix} 1 & 1 \\ ik_H & -ik_H \end{pmatrix}}_{M_1}\begin{pmatrix} A_2 \\ B_2 \end{pmatrix}$$

$$\underbrace{\begin{pmatrix} e^{-ik_Hd_2} & e^{ik_Hd_2} \\ ik_0e^{-ik_Hd_2} & -ik_0e^{ik_Hd_2} \end{pmatrix}}_{M_2}\begin{pmatrix} A_2 \\ B_2 \end{pmatrix}$$

$$= \underbrace{\begin{pmatrix} \sqrt{\xi_0}.J_{\frac{1}{4}}\left(\frac{\xi_0}{2\alpha}\right) & \sqrt{\xi_0}.Y_{\frac{1}{4}}\left(\frac{\xi_0}{2\alpha}\right) \\ -\xi_0\left(\frac{\alpha}{2\xi_0^{3/2}}.J_{\frac{1}{4}}\left(\frac{\xi_0}{2\alpha}\right)+\xi_0^{1/2}.J_{\frac{1}{4}}'\left(\frac{\xi_0}{2\alpha}\right)\right) & -\xi_0\left(\frac{\alpha}{2\xi_0^{3/2}}.Y_{\frac{1}{4}}\left(\frac{\xi_0}{2\alpha}\right)+\xi_0^{1/2}.Y_{\frac{1}{4}}'\left(\frac{\xi_0}{2\alpha}\right)\right) \end{pmatrix}}_{M_i}\begin{pmatrix} A_3 \\ B_3 \end{pmatrix}$$

… … … so on.

… … (2.6)

where $k_0(=\ (2\pi/\lambda).n_0.cos\theta_0)$ and $k_H(=\ (2\pi/\lambda).n_H.cos\theta_H)$ are the wave vectors of the incident (0^{th}) and homogeneous media, respectively. n_0 and θ_0 are refractive index and incident angle of the air (0^{th}) media, n_H and θ_H are refractive index and incident angle of the homogeneous media, respectively. In case of graded layers, wave vectors at the boundary of lower and higher refractive index are $\xi_0 = \omega.n_i.cos\theta_i/c$ and $\xi_1 = \omega.n_f.cos\theta_f/c$, where θ_i and θ_f are angle of incidence at boundary of lower (n_i) and higher (n_f) refractive index of the graded layer, respectively.

The expressions for the set of equations across the interface from one medium to the other are similar for both structures (Type1 and Type2) but their characteristic matrices will change according to the variation of refractive index in the graded layer. In the case of linearly increasing refractive index in the graded layers, wave vectors at

initial and final boundaries are $\xi_0 = \omega.n_i.cos\theta_i/c$ and $\xi_1 = \omega.n_f.cos\theta_f/c$ respectively. While the wave vectors at initial and final boundaries of the graded layer with linearly decreasing refractive index become $\xi_1 = \omega.n_f.cos\theta_f/c$ and $\xi_0 = \omega.n_i.cos\theta_i/c$, respectively. Here, n_f and n_i are refractive indices at initial and final boundary of the graded layers, respectively.

In order to investigate the propagation of electromagnetic wave in the periodic structures $(AB)^N$ and $(A'B)^N$, we have applied the transfer matrix approach. Thus, the electromagnetic waves propagation through the considered structure $(AB)^N$ can be expressed by multiplying the characteristic matrices of constituent layers (A and B) as;

$$\begin{pmatrix} A_0 \\ B_0 \end{pmatrix} = M_0^{-1}.(M_G.M_H)^N.M_0 \begin{pmatrix} A_{2n+1} \\ 0 \end{pmatrix} \quad \ldots\ldots \quad (2.7)$$

Similarly, the electromagnetic waves propagation through the structures $(A'B)^N$ can be expressed by multiplying the characteristic matrices of layers (A′ and B) as;

$$\begin{pmatrix} A_0 \\ B_0 \end{pmatrix} = M_0^{-1}.(M'_G.M_H)^N.M_0 \begin{pmatrix} A_{2n+1} \\ 0 \end{pmatrix} \quad \ldots\ldots \quad (2.8)$$

where N is the number of periods, A_0, B_0 and A_{2n+1} are the constant for incident (0^{th}) and outgoing $(2n+1)^{th}$ media, respectively. M_G and M'_G are 2×2 characteristic matrices for linearly increasing and decreasing refractive index layers, M_H and M_0 are 2×2 characteristic matrices of the homogeneous and air media, respectively. The characteristic matrices are $M_G = M_i.{M_f}^{-1}$, $M_H = M_1.{M_2}^{-1}$ and $M'_G = M_f.{M_i}^{-1}$, where M_i and M_f are characteristic matrices at lower and higher refractive index boundaries of the graded layers, $M_1$and M_2 are characteristic matrices at the initial and final boundaries of the normal layers, respectively. The characteristic matrices are given in the sets of matrix expressions for the interface from one medium to the other.

Now, we have considered the 1-D PC structure constituted a defect layer of linear graded index material. A schematic view of the structure with doping of a defect layer of linear graded index material is shown in figure 2.2, which composes a system of the form $(AB)^P ADA(BA)^P$, where P is the periodicity of the unit cells. The proposed structure is composed of two types of dielectric homogeneous layers as A and B, and a linear graded layer as defect (D). The relative refractive index of the layers A and B are assumed as n_A and n_B equal to 1.5 and 4.5, respectively. The defect layer D, which generates defect modes within the PBGs has been considered as a linear graded index

material. The refractive index of the graded layer varies in x-direction. The thickness of layers A, B and D are assumed to be a, b and d, respectively. The refractive index in the linear graded layer varies with the depth of layer.

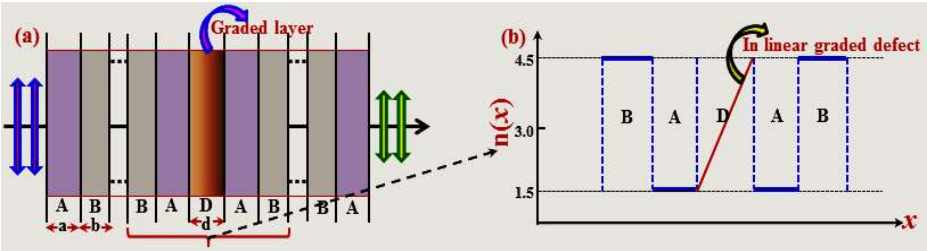

Figure 2.2 (a) Schematic representation of the structure with a linear graded defect layer form of $(AB)^{P}ADA(BA)^{P}$ with period P and (b) relative refractive index variation in centre unit cells.

Using the transfer matrix approach, the amplitudes A_0 and B_0 of the electromagnetic field in the air medium at $x<0$ are related to the amplitudes A_{n+1} and B_{n+1} of the $(n+1)^{th}$ medium through the linear transformation. Therefore, for the proposed multilayer structures, the total transfer matrix equation can be written as;

$$\begin{pmatrix} A_0 \\ B_0 \end{pmatrix} = M_{i,j} \cdot \begin{pmatrix} A_{n+1} \\ B_{n+1} \end{pmatrix} \quad \ldots\ldots \quad (2.9)$$

where $M_{i,j}$ $(i, j = 1,2)$ is the total characteristic matrix and if atmosphere around the system is air, $M_{i,j} = M_0^{-1}.(M_1 \text{ x } M_2 \text{ x } M_3 \text{ ... x } M_n).M_0$ for the n layer system and M_n is the characteristic matrix of n^{th} layer. Layers may be homogenous or linear graded materials.

If the electric field is known at the beginning of a system, the field at the end of the same system can be derived from a simple matrix operation as given in the above sets of matrix equations. A stack of layers can then be represented as a complete system matrix. In this way, the reflection (r) and transmission (t) coefficients of the fields in the incident and outgoing media can be directly obtained. Therefore, reflectance (R) and transmittance (T) of the structures are determined using the following relations:

$$R = |r|^2 = \left|\frac{B_0}{A_0}\right|^2 \text{ and } \quad T = |t|^2 = \left|\frac{A_{N+1}}{A_0}\right|^2 \ldots\ldots \quad (2.10)$$

According to the Floquet's theorem, the electric field vector of a normal mode of propagation in a periodic medium takes the form as; $E_K(x,z) = E_K(x).e^{-i.\beta.z}.e^{-i.K.x}$, where $E_K(x)$ is a periodic function with period d, i.e. $E_K(x+d) = E_K(x)$ and β is the z component of the wave vector. This optical wave is known as Bloch mode and the

parameter K, satisfying the mode and its associated a periodic function $E_K(x)$ is called the Bloch wave number. The dispersion relation is given by

$$\boldsymbol{K(\beta,\omega) = \frac{1}{d}\,.cos^{-1}\left\{\frac{1}{2}(M_{11} + M_{22})\right\}} \quad \ldots\ldots \quad \textbf{(2.11)}$$

where d is the total thickness of a period of the periodic system, M_{11} and M_{22} are the elements of 2×2 optical transfer matrix $M_{ij}(i,j=1,2)$. The optical transfer matrix for the structure composed of a linear graded layer A and A′ are $M_{ij} = (M_G.M_H)^N$ and $M_{ij} = (M'_G.M_H)^N$, respectively.

The dispersion relation exhibits multiple spectral bands classified in two regimes. When $|(M_{11} + M_{22})/2| \leq 1$, K is real and corresponds to propagating Bloch waves. On the other hand, if $|(M_{11} + M_{22})/2| > 1$, K becomes complex which results in evanescent waves that are rapidly attenuated. These bands correspond to the stop bands of the systems known as photonic band gaps or forbidden gaps since propagating modes do not exist [Yeh (1988)].

2.3 Numerical Results and Discussion

In this section, we have first presented the numerical results regarding optical reflection, band structures, phase shift and omnidirectional band gap obtained for 1-D GPC structures as shown in figure 2.1. The medium B is considered as homogeneous layer of refractive index n_B and the medium A or A′ are taken as linear graded index layer. In the graded layer, the refractive index linearly varies with layer thickness in increasing (for layer A) or decreasing (for layer A′) fashion between lower refractive index $n_i = 1.5$ and higher refractive index $n_f = 4.5$. Next, the photonic band gap and defect mode properties at different structural and material parameters in the 1-D PC structure with a defect layer of linear graded index material have investigated. In these studies, we have assumed that the light incident on the structure through air and materials are lossless dielectric. Our observations for the considered 1-D PC structures with linear graded index materials have been carried out in the following steps.

2.3.1 Effect of layer thickness on photonic band gaps

First, the reflection spectra of 1-D GPC structures at different layer thickness for selected refractive index of homogeneous layer B under the normal incident angle have been presented. Thickness of the homogeneous and graded layers are chosen as to give; $n_B d_2 = n_m d_1 = D$, where n_m is the mean value of n_i and n_f. Thickness of a

graded and homogenous layers considered as $d_1$and d_2 respectively with a total thickness $d = d_1 + d_2$. For the various layer thickness, D choose as $q \times \lambda_0/4$, where q is the integral multiplier as 1, 2, 3… and λ_0 is the optical wavelength equal to the wavelength of the mean value of the considered frequency range (200 – 800 THz).

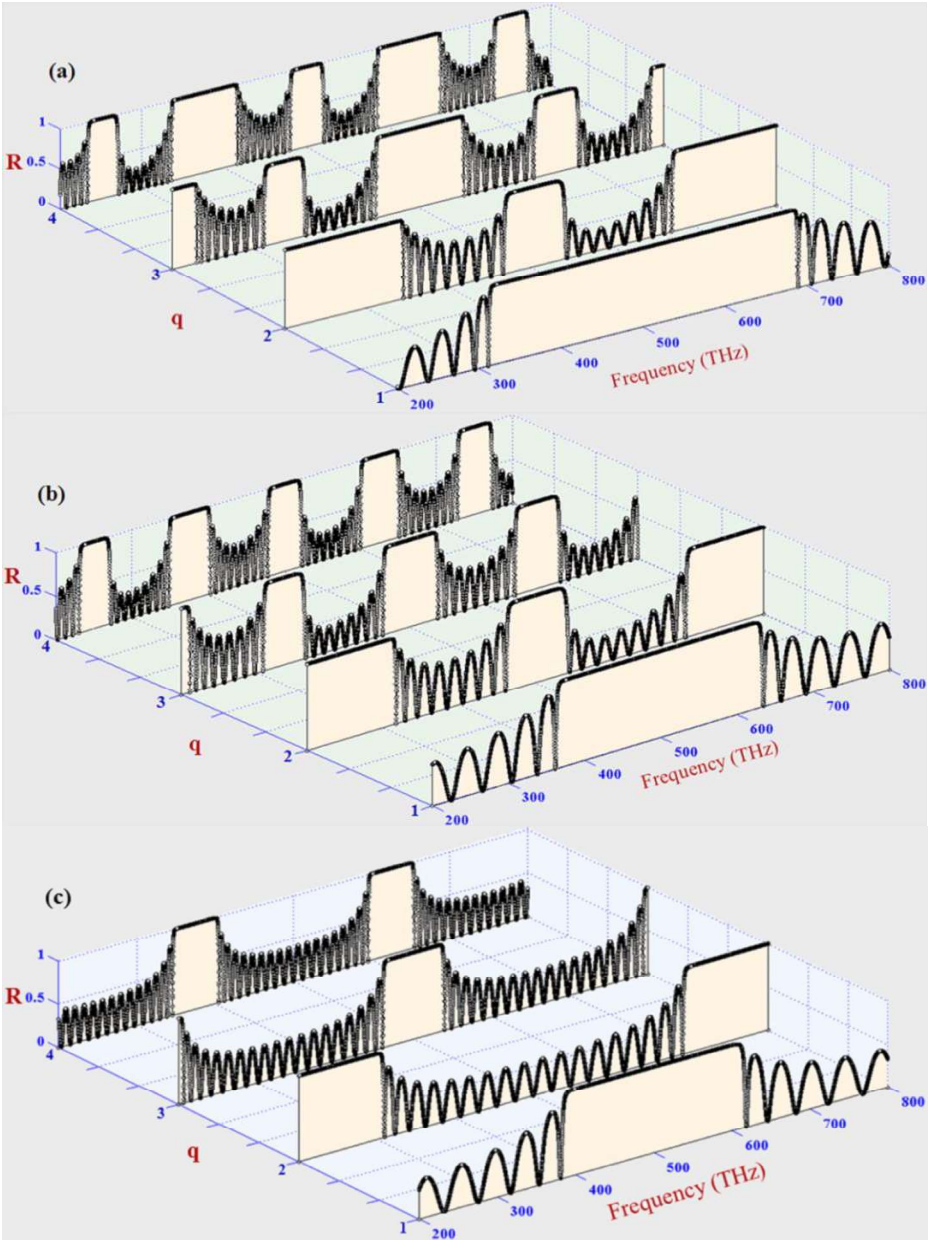

Figure 2.3 Reflectance spectra of the considered 1-D GPC structures for the refractive index (a) n_B = 1.0 and (b) n_B = 1.5 with various layer thickness coefficient D ($= q\lambda_0/4$). Panel (c) shows the reflection spectra for the structure with uniform refractive index of layer A and B equal to 1.5 and 3.0, respectively.

It is evident from the results shown in figure 2.3 that a number of photonic bands are generated. The number of PBGs increases with layers thickness. The average

refractive index over the volume of each graded layer becomes larger as the increase of layers thickness. As the results, the refractive index contrast between the two constituted layers is enhanced that influences the continuous interference effectively. We observed that the reflection spectra remain unchanged for the structures with linear graded layer A or A′. Figures 2.3(a) and 2.3(b) respectively show the reflection spectra of the structures for the constituted homogeneous layer refractive index n_B equal to 1.0 and 1.5. For different refractive indices of homogeneous layer B, the formation of photonic bands is similar under normal angle of incidence, but their bandwidths become larger for $n_B = 1.0$ as compared to the other values of n_B. PBG properties are basically modulated by the contrast between refractive index of constituted media. For the structure with $n_B = 1.0$, the contrast of refractive index between homogeneous and graded layer is higher as compared to the other. Therefore, the Bragg stack is more effective to producing the wider width of photonic bands. Figure 2.3(c) shows the reflection spectra for the structure with uniform refractive index layer in place of graded index layer and refractive index for the layer A and B would be considered the values 1.5 and 3.0, respectively. In this case, PBGs do not continuously increase with layer thickness. The number of band gaps and corresponding bandwidth are also small.

Next, we examine the confinement effects arising from competition between the structures induced by changing the thickness of layers and magnitude of the total photonic bandwidths in the PBG spectra for the considered structures under the normal angle of incidence. To do that, we calculate the regions for forbidden frequencies (stop bands), where $|(M_{11} + M_{22})/2| > 1$, as a function of the thickness of layers and depicted in figures 2.4(a) and 2.4(b) for the structures with n_B equal to 1.0 and 1.5, respectively. These figures show the distribution of the forbidden (black region) and allowed (white region) frequency regions as a function of the thickness of layer up to the value of D = 9×λ_0/4. Thickness of layers varies in the form $n_m\, d_1 = n_B\, d_2 = D$, where D = q×$\lambda_0$/4 (q = 1, 2, 3…9). As expected, the forbidden band gaps observed at zero transmission intensity range and increases with increasing the thickness of layers i.e. increasing the value of q. Also as once again seen here, number of photonic bands increases with the layers thickness, single band observe for the layer thickness proportional to λ_0/4 (q=1), three bands for the layer thickness proportional to λ_0/2 (q=2), and similarly for other cases. The bandwidths of PBGs become narrow and narrow as increasing the number of photonic bands. The corresponding total PBG variations at

various layer thicknesses for the finite crystals are depicted in figure 2.4(c) for the different refractive indices of the layer B. Here, total PBG represents the addition of the forbidden band widths for the structures at different considered layer thickness as the form $n_m\ d_1 = n_B\ d_2\ = D$, where D = q×λ₀/4 (q = 1, 2, 3…9).

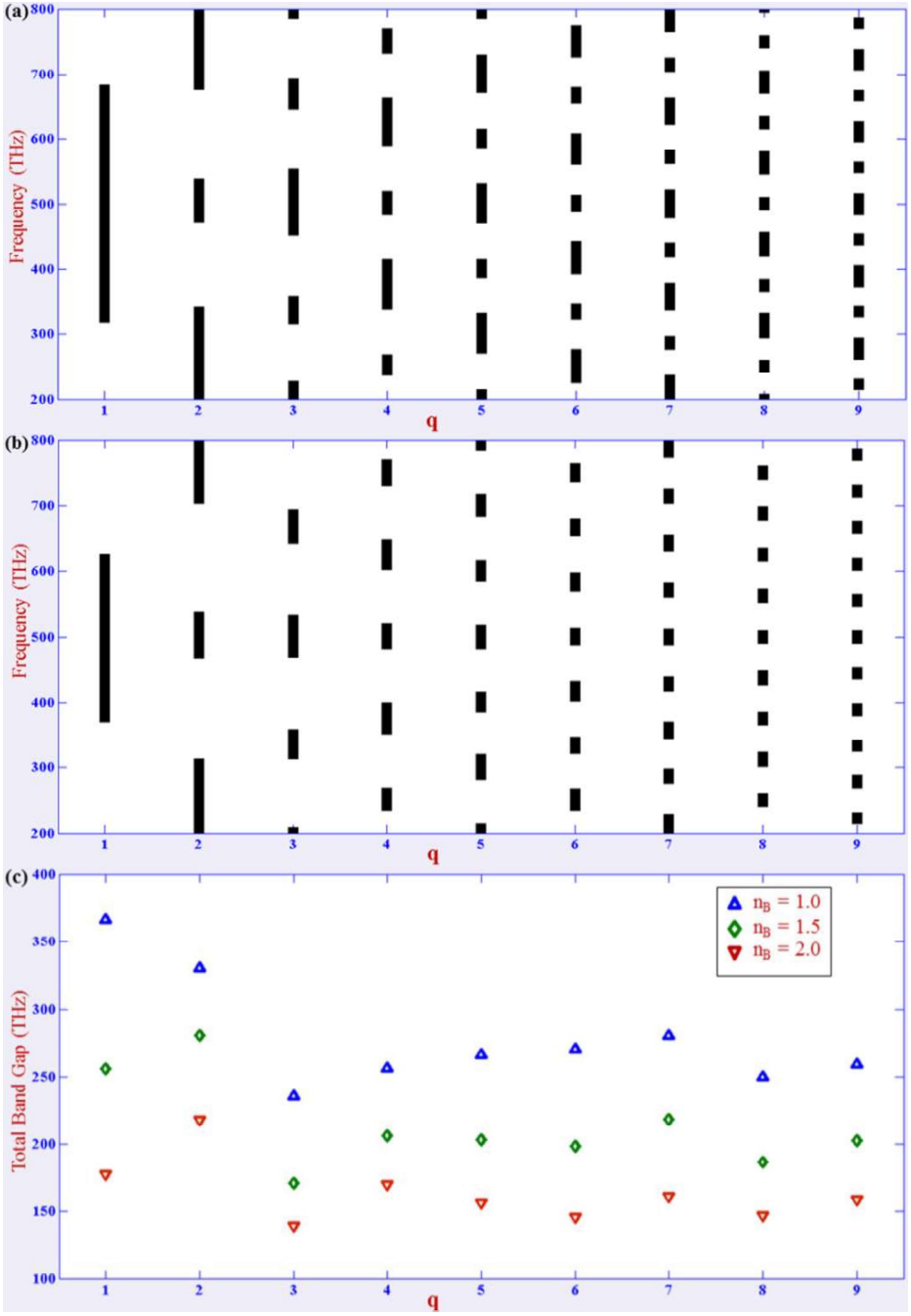

Figure 2.4 The distribution of bandwidth of photonic band gaps as a function of the layer thickness constant D for the structures with homogenous layers refractive index (a) $\boldsymbol{n_B}$ = 1.0, and (b) $\boldsymbol{n_B}$ = 1.5, and plot (d) shows the total band gap of the forbidden band regions against the layer thickness constant D ($= \boldsymbol{q}\times\boldsymbol{\lambda_0/4}$).

It reveals that the total band gap randomly varies with increasing the layers thickness, but that is maximum for the quarter-wave (q = 1.0) stacked structures with $n_B = 1.0$, while in the structures with $n_B = 1.5$ and $n_B = 2.0$, total band gap is maximum for the latent (q = 2.0) type layer stacking arrangement. Therefore, the number of photonic bands and their frequency region can be tuned by adjusting the layers thickness and refractive index of the constituted homogeneous layers. The forbidden band regions and their bandwidths at different layer thicknesses and various refractive index of acceptably homogeneous layer (B) are listed in Table 2.1.

Table 2.1. Reflection band region and bandwidth of the considered 1-D GPC structures at different layer thickness under normal angle of incidence.

Layer thickness constant (D)	Structures with $n_B = 2.0$		Structures with $n_B = 1.5$		Structures with $n_B = 1.0$	
	Reflection Band Region (nm)	Reflection Bandwidth (nm)	Reflection Band Region (nm)	Reflection Bandwidth (nm)	Reflection Band Region (nm)	Reflection Bandwidth (nm)
$\lambda_0/4$	585.2 – 408.2	177	626.0 – 370.4	255.6	683.5 – 317.1	366.4
$\lambda_0/2$	292.6 – 204.2	88.4	313.0 – 200.0	113	341.6 – 200.0	141.6
	537.6 – 465.4	72.2	538.2 – 468.2	70	538.0 – 473.0	65
	778.8 – 722.0	56.8	750.0 – 702.8	47.2	800.0 – 676.2	123.8
$3\lambda_0/4$	358.4 – 310.2	48.2	208.6 – 200.0	8.6	227.8 – 200.0	27.8
	519.2 – 481.4	37.8	358.8 – 312.2	46.6	358.6 – 315.4	43.2
	693.6 – 640.6	53	533.6 – 468.6	65	553.6 – 450.8	102.8
			693.6 – 642.2	51.4	692.8 – 645.2	47.6
					800.0 – 785.8	14.2
λ_0	268.8 – 232.8	36	269.0 – 234.2	32.4	269.0 – 236.6	32.4
	389.4 – 361.0	28.4	400.2 – 351.4	48.8	415.2 – 338.2	77
	520.2 – 480.6	39.6	520.2 – 481.8	38.4	519.6 – 483.8	35.8
	637.4 – 613.0	24.4	648.2 – 603.0	45.2	663.4 – 589.4	74
	770.6 – 729.8	40.8	770.6 – 730.8	39.8	769.8 – 732.8	37

Due to the importance of the widespread PBGs for the proposed structures, we would like to extend the study on the dispersion curves and reflection phase shift associated with the wider PBGs in the structures with $n_B = 1.0$. For different layer thicknesses, dispersion curves are calculated from equation (2.11) for the unbounded periodic structures and shown in panels (i) of figure 2.5 as functions of the reduced Bloch wave vector kd/π, and related reflection phase shifts are likewise illustrated in panels (ii) and (iii) for the structures $(AB)^{10}$ and $(A'B)^{10}$, respectively. As expected, the band gaps observed at zero transmission intensity range. The corresponding dispersion curves for the finite crystal are depicted in the panels (i) of figure 2.5(a) and 2.5(b)

respectively for layers thickness with relative refractive index equal to $\lambda_0/4$ and $\lambda_0/2$. Also as seen here, the number of bands increases with the layers thickness, single band formed for layer thickness with relative refractive index equal to $\lambda_0/4$ and three bands for $\lambda_0/2$, but the bandwidths of forbidden bands as expected become narrow and narrow with increasing the number of bands.

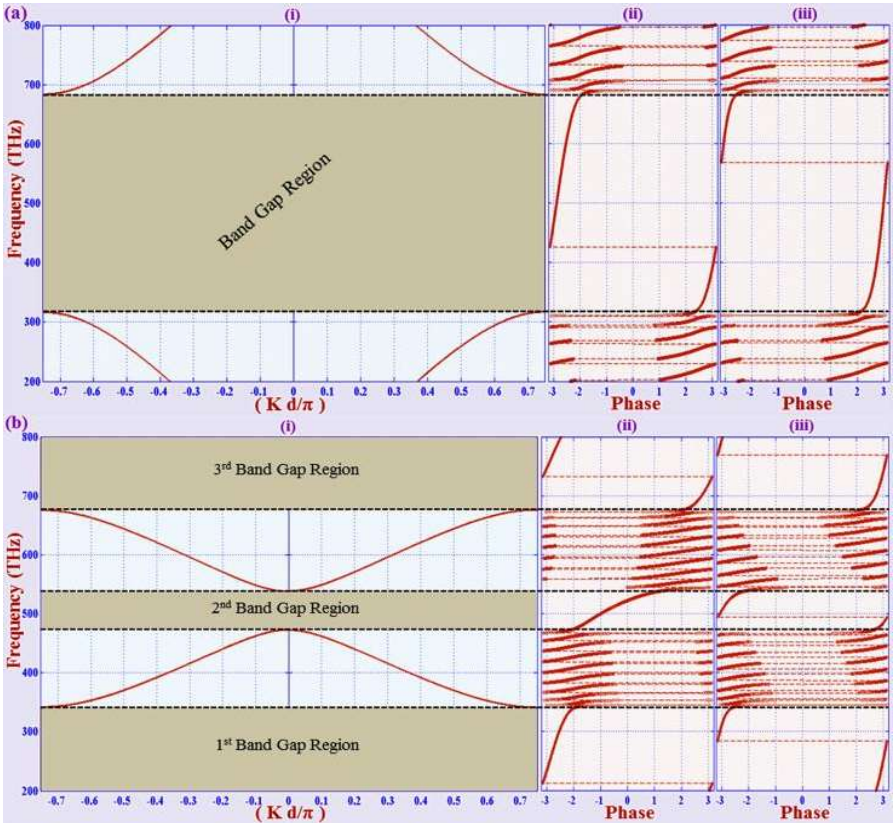

Figure 2.5 Panel (i) shows the dispersion spectra for both types of considered periodic arrangements for optical layer thickness with relative refractive index equal to (a) $\lambda_0/4$, and (b) $\lambda_0/2$, while panels (ii) and (iii) illustrate the reflection phase shift of the structures $(AB)^{10}$ and $(A'B)^{10}$, respectively and $\boldsymbol{n_B = 1.0}$.

The reflection phase shifts are shown in panels (ii) and (iii) of the figure 2.5 for the structures $(AB)^{10}$ and $(A'B)^{10}$, respectively. It can see that the variations of the reflection phase shifts are slightly different within the bang gap regions. Distribution of field changes according to the gradation profiles. Therefore, due to the transform of field intensities distribution at the interface boundaries, the phase shifts are change between $+\pi$ and $-\pi$ with different values. According to above results, reflection, transmission and PBG spectra are independent on the arrangement (AB or A'B) of layers in unit cells of the structures, while reflection phase shifts change with arrangement of layers in the unit cells of the structures.

For a better understanding of the effect of layer arrangements in 1-D GPCs, we have computed the spatial distribution of the squared magnitude of the electric field E(x) at selected frequencies for 0%, 50% and 100% reflection conditions in the structures $(AB)^{10}$ and $(A'B)^{10}$. The results are shown in the figure 2.6.

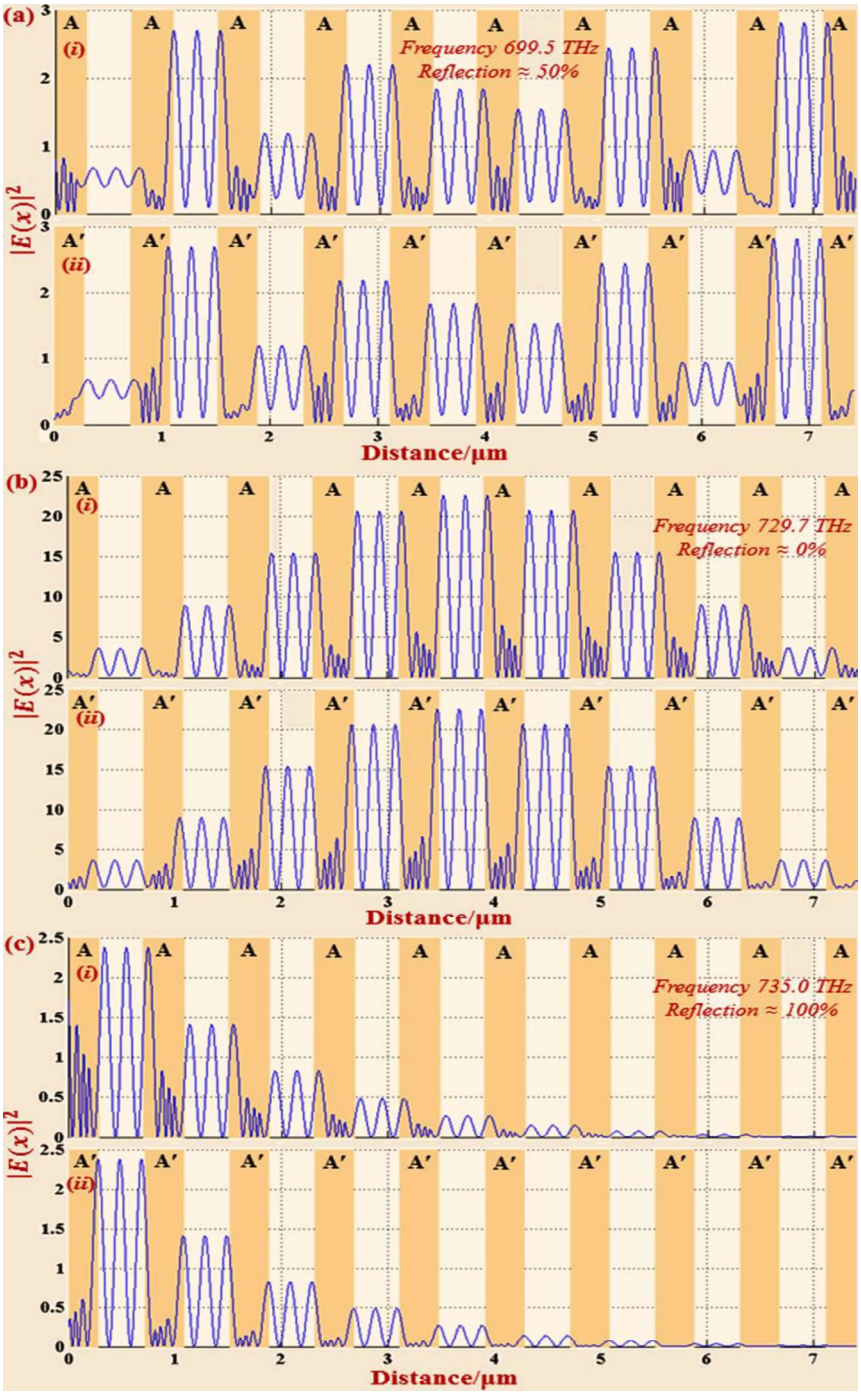

Figure 2.6 Distributions of electric field intensity in the systems $(AB)^{10}$ and $(A'B)^{10}$ respectively show in panels (i) and (ii) at three selected frequencies (a) 699.5 THz, (b) 729.7 THz, and (c) 735 THz impinging under ≈50%, ≈0% and ≈100% reflection.

The effect of grading on electric field is substantially visible with the computed values of the thickness of layers for λ_0 (= 600 nm). In figure 2.3(a), we seen that a spectral band edge position at frequency 729.7 THz (where close to 0% reflection), and reflection is stronger ≈100% within the band gap region observed for frequencies 735 THz. It is to be noted that one of the peak occurs at 699.5 THz shows ≈50% reflection. Therefore, electric field intensities within the structures $(AB)^{10}$ and $(A'B)^{10}$ for frequencies 699.5 THz, 729.7 THz, and 735 THz are shown in figures 2.6(a), 2.6(b) and 2.6(c) respectively. Panels (i) and (ii) of the figure 2.6 show the distribution of electric field intensity in the periodic structures $(AB)^{10}$ and $(A'B)^{10}$ respectively. It is found that the electric field distributions in linear graded layers for different grading profiles are different, although the volume-average refractive index remains same. The electric field intensities decrease in graded layers A while it increases in graded layers A′ along the propagation depth as can see in panels (i) and (ii), respectively. The electric field intensities in non-graded layers are found to be unchanged for both types of the structures $(AB)^{10}$ and $(A'B)^{10}$.

2.3.2 Study of the omnidirectional band gap (OBG)

In this section, the omnidirectional band gap (OBG) characteristics of the proposed structures with layers arrangement in quarter-wave stacking have discussed. An OBG can be obtained within a specific frequency range as a forbidden band gap, if forbidden band gap reflects the electromagnetic wave incident at any incident angle for both TE and TM-polarization. Dependence of the PBG on the incident angle is shown in figures 2.7(a and b) and 2.8(a and b) for the structures with refractive index n_B equal to 1.5 and 2.0, respectively. These figures clearly demonstrated the expansion of PBG for both TE and TM-wave in the structures with n_B = 1.5 and 2.0. In case of the structure with n_B = 1.0, PBG spreading in frequency for TE-wave and shrinking in frequency for TM-wave, when angle of incidence increases. In order to discuss the OBG properties of the structures, the projection band spectra as changing of the incident angle have plotted in figures 2.7(c) and 2.8(c), respectively for the structures with n_B = 1.5 and 2.0. From the figures, it can clearly inspect the variation of higher and lower band edges as changing of the incident angle. There is an OBG exists between higher and lower band edges as prevalent band region for both TE and TM-polarization. The photonic band structure can be usually achieved from the projection of unit reflectance. In figures 2.7(c) and 2.8(c), the dark area represents the photonic band region and the white area

between the band edges that is ubiquitous in both TE and TM polarizations illustrates the OBG. The Omni-directional band range and bandwidth of the structures for different n_B-values are tabulated in Table 2.2.

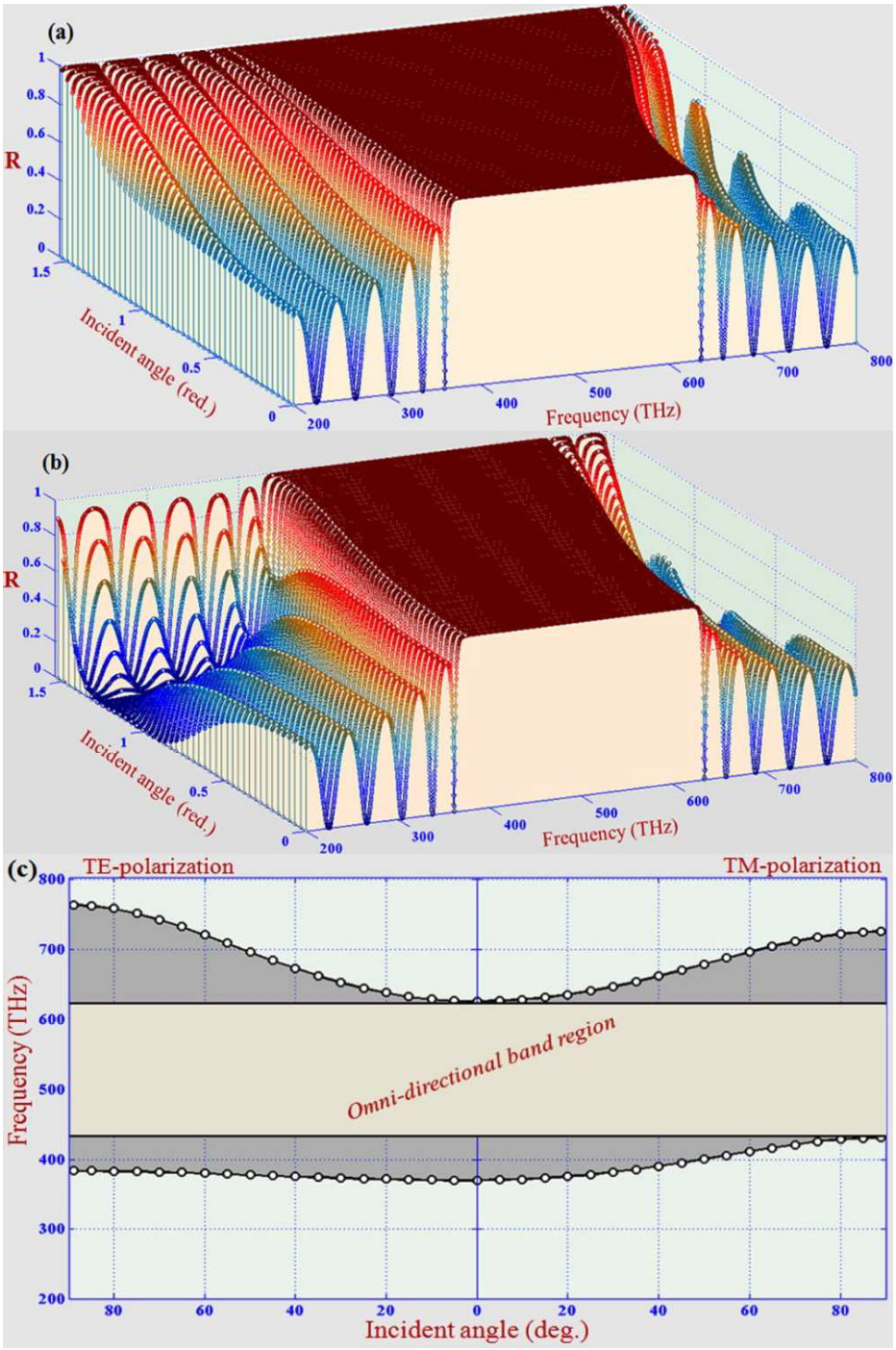

Figure 2.7 Reflection (R) spectra for (a) TE-polarization, (b) TM-polarization and (c) projected reflection band structure as changing of the incident angle for the quarter-wave type layer stacking arrangement in the considered structure with n_B = 1.5.

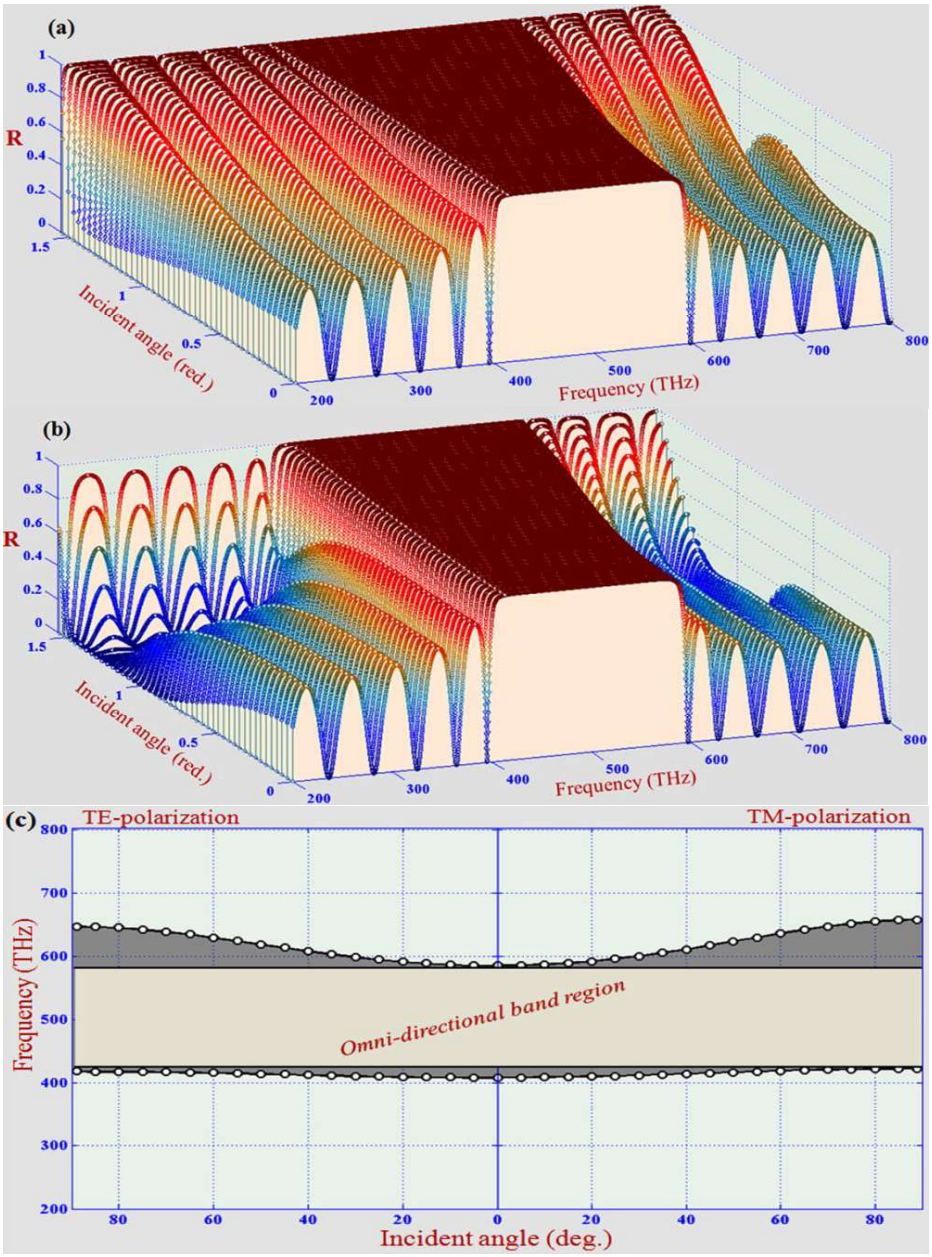

Figure 2.8 Reflection (R) spectra for (a) TE-polarization, (b) TM-polarization and (c) projected reflection band structure as the changing of the incident angle for the quarter-wave type layer stacking arrangement in the considered structure with n_B = 2.0.

Table 2.2 Omnidirectional band region and bandwidth of the considered GPC structures with quarter wave layer stacking.

Structures with layer B refractive index	Complete Band Region in		Omni-directional Band Region (nm)	Omni-directional Band Width (nm)
	TE-polarization	TM-polarization		
$n_B = 2.0$	585.2 – 418.0	585.2 – 422.0	585.2 – 422.0	160.2
$n_B = 1.5$	626.0 – 384.0	626.0 – 431.4	626.0 – 431.4	194.6
$n_B = 1.0$	683.4 – 335.6	…….	…….	…….

It is certified from the table 2.2, an Omni-directional band exists for structures with n_B = 1.5 and 2.0, while it is not exist in the structures with n_B = 1.0. Nevertheless, one obvious feature of the structures with n_B = 1.0 is that there exist broadest complete band gap for TE-wave. Therefore, the structures with n_B = 1.0 is more suitable for design TE-polarized photonic devices while structures with n_B = 2.0 and 1.5 can be used for design omnidirectional photonic devices. Here, we also observe that the existence of omnidirectional bands affected by the contrast of the refractive index of the homogeneous and graded layer. In latent type layer stacking structures, we observe the number of omnidirectional bands exists for the structures with n_B = 2.0 and 1.5, and it is absence for the structures with n_B = 1.0. Therefore, these types of structures can be used to utilize the widespread omnidirectional photonic devices in multiple omnidirectional frequency regions.

2.3.3 Effect of the contrast of n_i and n_f on the photonic band gap

The dependence of the PBG on the contrast of initial and final refractive indices i.e. $(n_f \sim n_i)$ of the linear graded index layer under normal incidence in the proposed structures with different layer thicknesses has been demonstrated. Here, we have taken the fixed refractive index n_i of 1.5, while refractive index n_f varies according to the contrast values. First, the reflection coefficients for a quarter-wave stacked structures with $n_B = 1.0$ at different values of $(n_f \sim n_i)$ have calculated and depicted in figure 2.9(a). Second, the demonstration of reflection spectra at different values of $(n_f \sim n_i)$ for the structures with precise layer thickness d_1 = 60 nm and d_2 = 90 nm are shown figure 2.9(b). It found that the photonic bandwidth decreases with $(n_f \sim n_i)$. The rate of change of grading profile parameter (α or α') decreases and corresponding average refractive index over the volume of each graded layer also decreases with decreasing the value of $(n_f \sim n_i)$. Hence, the Bragg effect becomes less effective. For a quarter-wave stacked structures, reflection spectra are approximately symmetrical around the central frequency as shown in figure 2.9(a), while for the structure with layer thickness d_1 = 60 nm and d_2 = 90 nm, band gap region is shifted towards higher frequency as shown in figure 2.9(b). Accordingly, the photonic bandwidths and their frequency region can tune by adjusting the grading profile parameters and layer thicknesses.

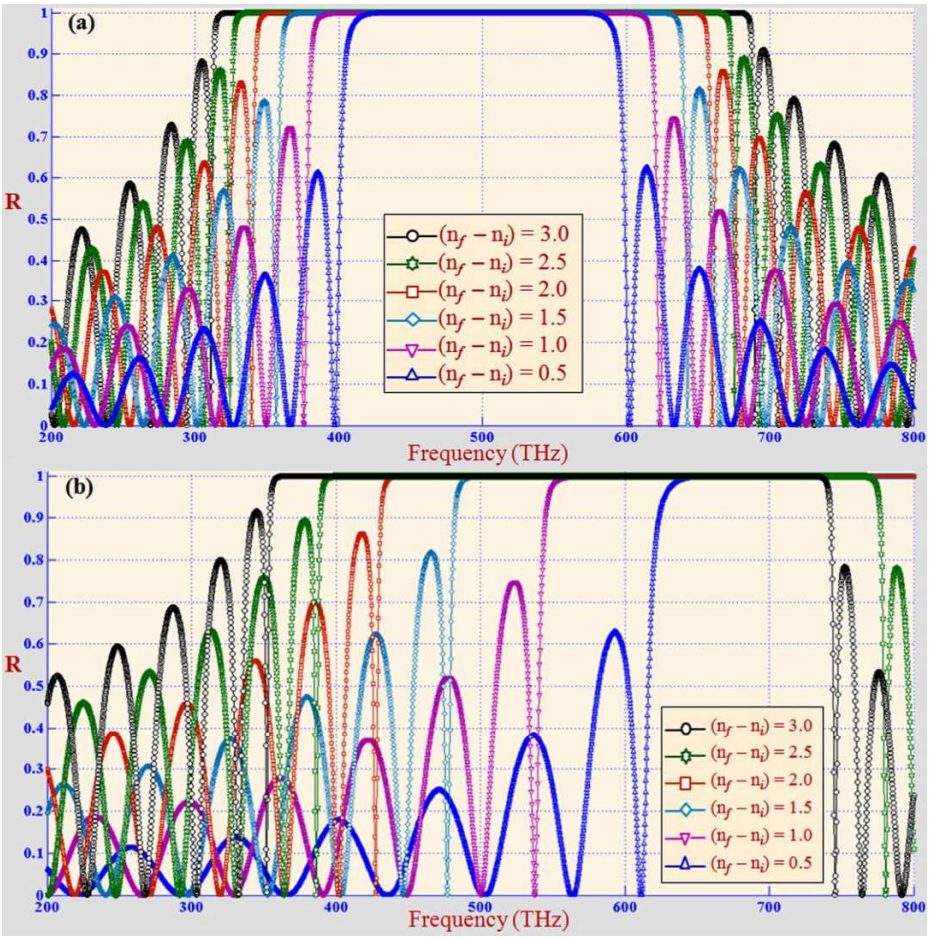

Figure 2.9 Reflectance spectra for different values of the contrast between initial ($\boldsymbol{n_i}$) and final ($\boldsymbol{n_f}$) refractive index of linear graded index layer in the considered 1-D GPC structures with (a) quarter-wave layer stacking and (b) precise layer thickness; $d_1 = 60$ nm and $d_2 = 90$ nm arrangements, and parameters; $\boldsymbol{n_i = 1.5}$ and $\boldsymbol{n_B = 1.0}$.

Moreover, we have plotted the forbidden bandwidths as changing the contrast $(n_f \sim n_i)$ for the structures with different layers thickness arrangements under normal angle of incidence, which are illustrated in the figure 2.10. Figure shows the variation of photonic bandwidth as a function of $(n_f \sim n_i)$ for the structures with different layer thicknesses. Bandwidth of photonic bands increases linearly with $(n_f \sim n_i)$ for a quarter-wave type layer stacking structures. For other types of the structures with precise layer thickness, the bandwidth photonic bands initially increase linearly with $(n_f \sim n_i)$ up to 1.5. However, the bandwidths are deviated slightly from its linear trend and become approximately constant above to the contrast value 1.5. The band ranges and bandwidths of PBGs of the considered 1-D GPC structures with different layer thicknesses are tabulated in Table 2.3.

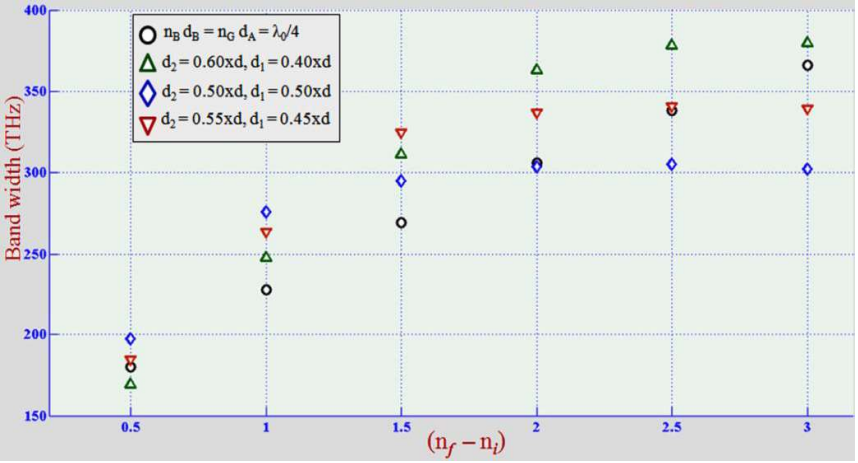

Figure 2.10 The variations of bandwidth of photonic band gaps as a function of the contrast value $(\boldsymbol{n_f \sim n_i})$ for different layer thickness arrangement in the considered structures with homogenous layers refractive index equal to 1.0, here $\boldsymbol{n_i = 1.5}$ and d = 150 nm.

Table 2.3 Reflection band region and bandwidth for different values of contrast $\boldsymbol{(n_f - n_i)}$of the considered 1-D GPC structures at normal incidence, and $\boldsymbol{n_i = 1.5}$ and d = 150 nm.

$(n_f - n_i)$	Structure with quarter wave stacking		Structure with constant layers thickness					
			$d_1 = 0.40*d$ and $d_2 = 0.60*d$		$d_1 = 0.45*d$ and $d_2 = 0.55*d$		$d_1 = 0.50*d$ and $d_2 = 0.50*d$	
	Band Range (nm)	Width (nm)	Band Range (nm)	Width (nm)	Band Range (nm)	Width (nm)	Band Range (nm)	Width (nm)
0.5	589.8−409.8	180	800.0−630.8	169.2	800.0−615.4	184.6	800.0−602.8	197.2
1	613.4−386.0	227.4	800.0−552.2	247.8	800.0−536.4	263.6	799.0−523.4	275.6
1.5	634.2−365.0	269.2	800.0−488.6	311.4	797.4−473.0	324.4	755.2−460.2	295
2	652.6−346.8	305.8	800.0−437.0	363	758.8−422.0	336.8	713.4−409.6	303.8
2.5	669.0−331.0	338	772.8−394.6	378.2	721.2−380.4	340.8	673.8−368.6	305.2
3	683.4−317.2	366.2	738.8−359.2	379.6	685.0−345.8	339.2	636.8−334.6	302.2

Accordingly, the average refractive index over the volume of each layer and the different grading profile parameters have great influence on the photonic and omnidirectional band gaps, reflection phase shift and electric field distribution in the 1-D GPC structures. Our investigations clearly demonstrate that the several structural parameters are accessible to tune the desirable photonic and Omni-directional band gaps in the 1-D GPC structures.

2.3.4 Photonic band gap and defect mode in one-dimensional photonic crystal with defect layer of linear graded index material

Now, we present the numerical results to characterize the PBG spectra and defect modes due to the defect layer of the linear graded index material in the 1-D PC

structures of the form $(AB)^P ADA(BA)^P$, where P is the periodicity of the unit cells. We have considered medium A and B as a homogeneous dielectric layer of refractive index 1.5 and 4.5, respectively whereas medium D is a defect layer having linear grading index profile. Linear grading profiles are considered to be varying refractive index with depth of the graded layer in increasing fashion between lower refractive index $n_i = 1.5$ and higher refractive index $n_f = 4.5$, as expressed by equation (2.1). The refractive indices of homogeneous and graded index materials are assumed to maintain the large refractive index contrast for better appearances of the grading effect on the PBG and defect modes. An enumerable number of materials are available whose refractive index exists in the considered range. In this study, we assume that light incident through the air medium and layered materials are lossless dielectric. Analysis is carried out mainly in two parts. Firstly, the effect of defect layer parameters on the transmission spectra and defect modes for the structure are studied. Moreover, distributions of the electric field in such PCs are computed. Secondly, the effect of incident angles on the transmission spectra and defect modes in the structure for TE and TM-polarization have been investigated. The changing of defect mode frequency and intensity as a function of the incident angle are also analysed.

As mentioned above, the arrangement of the layers has been taken in the form of $(AB)^P(ADA)(BA)^P$. Defect layer D represents of the linearly varying refractive index between initial refractive index n_i and final refractive index n_f as a function of the depth of graded layer. The transmission spectra of the structures without defect and with a defect layer of the graded index material for different periodicity P are shown in the figures 2.11(a) - 2.11(c). Thicknesses of the layer A, B and D are chosen in terms of quarter-wave stacked i.e. $n_A a = n_B b = n_m d = \lambda_0/4$, where a, b and d are the thickness of layers A, B and D, respectively and n_m is the mean value of the initial and final refractive index of the graded layer. These types of stacked structures are very useful and suitable for designing various photonic devices because they provide wider PBG and symmetrical reflection spectra around the centre frequency. The physical parameters used here are $n_A = 1.5, n_B = 4.5, n_m = 2.5$ and λ_0 (600 nm) is the mean value of the considered frequency region (200 – 800 THz). The transmission spectrum of the mirror symmetry structure of the form $(AB)^6AA(BA)^6$ is shown in the panel (a) and the transmission spectra of the structure to compose a defect layer in the form $(AB)^P ADA(BA)^P$ for period (P) equal to 6 and 7 are shown in the panels (b) and (c) of

the figure 2.11, respectively. These figures show that there exists single defect mode for the structure without defect layer while two defect modes exist in the forbidden band gaps for the structure with graded index defect layer. The defect mode of the structure without defect layer exists at the central frequency (500 THz), while in the case of structure with defect layer, first and second defect modes exist at lower and higher frequency side to the central frequency, respectively. The position of first defect modes is slightly shifted toward higher frequency and position of second defect mode shifted toward lower frequency with increasing the periods. The defect mode intensities also change with periodicity.

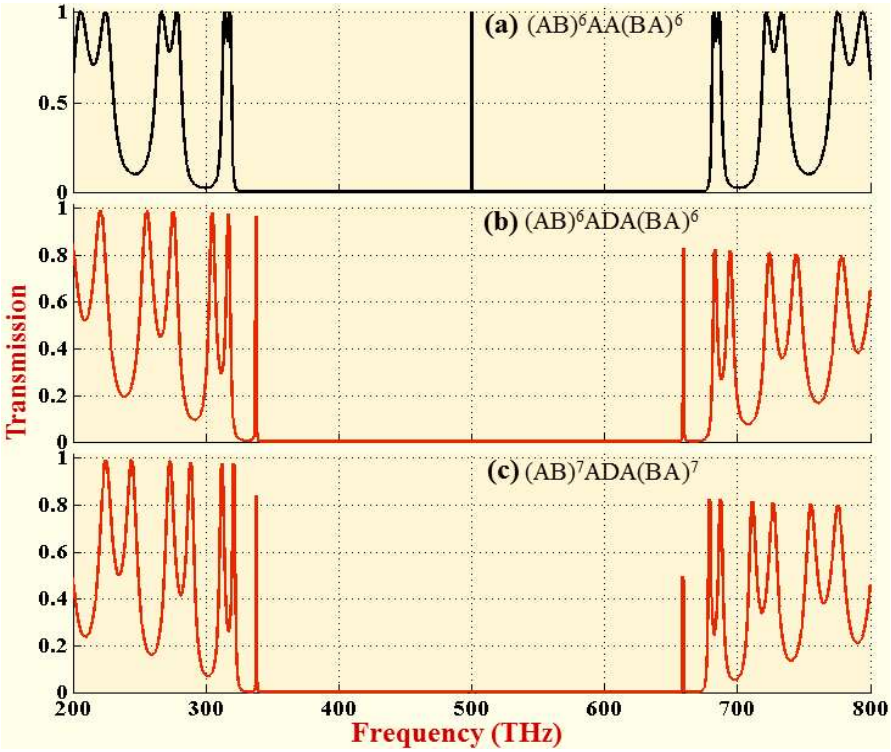

Figure 2.11 Transmission spectra of the structure (a) $(AB)^6AA(BA)^6$, (b) $(AB)^6ADA(BA)^6$ and (c) $(AB)^7ADA(BA)^7$. Here, refractive indices: $\boldsymbol{n_A = 1.5}$, $\boldsymbol{n_B = 4.5}$, $\boldsymbol{n_i = 1.5}$ and $\boldsymbol{n_f = 4.5}$, and thickness: $[\boldsymbol{n_A.a = n_B.b = n_m.d = \lambda_0/4}]$, where λ_0 = 600 nm and $\boldsymbol{n_m = (n_i + n_f)/2}$.

For better understanding the effect of periodicity (P) of unit cells on the defect modes frequency (f_D) and defect mode intensity in the structure $(AB)^PADA(BA)^P$, we have demonstrated the dependence of defect mode frequency (f_D) and defect mode intensity on the period P in the figure 2.12. The defect mode frequencies of the first and second defect modes slightly change the position with increasing the periodicity as depicted in the figure 2.12(a). The changing of defect mode frequencies with increasing

the period P become smaller and smaller. The intensities of the first defect mode are high as compared to second defect mode intensity as shown in figure 2.12(b).

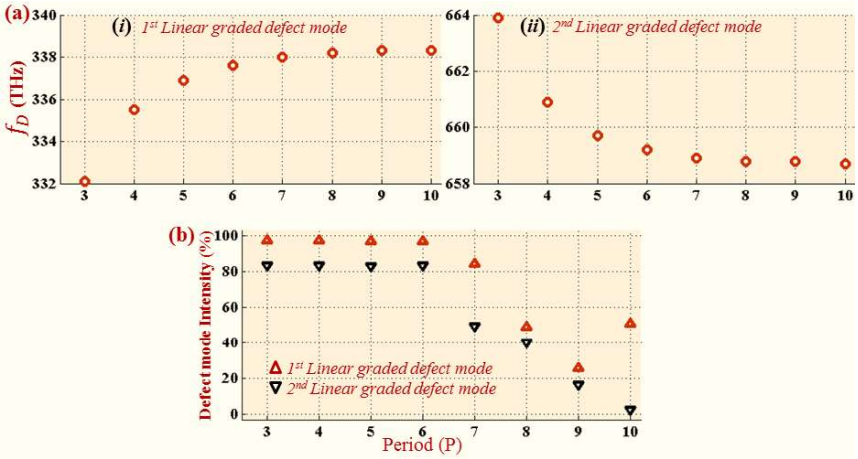

Figure 2.12 The dependence of (a) defect mode frequency ($\boldsymbol{f_D}$) and (b) defect mode intensity on the period (P) in the structure of the form $(AB)^P ADA(BA)^P$ containing linear graded index material as defect layer D.

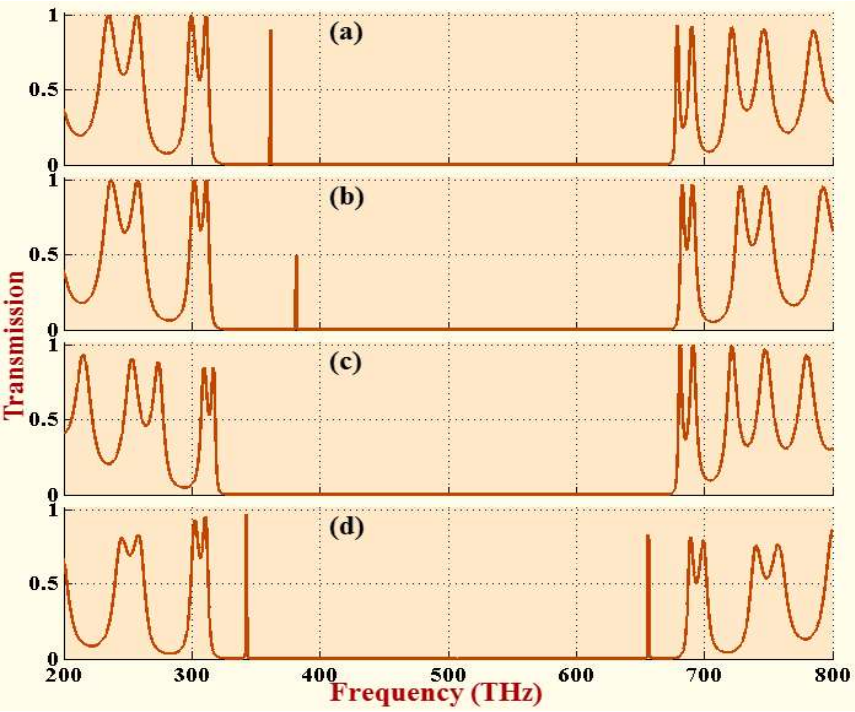

Figure 2.13 Transmission spectra of the defect modes of $(AB)^5 ADA(BA)^5$ at different thickness of defect layer D. The refractive indices: $\boldsymbol{n_A = 1.5}$, $\boldsymbol{n_A = 4.5}$, $\boldsymbol{n_i = 1.5}$ and $\boldsymbol{n_f = 4.5}$. Case of (a) thickness of defect layer D equal to thickness of layer B, (b) thickness of defect layer D = 25 nm, (c) thickness of defect layer D = 100 nm and (d) thickness of defect layer D = 200 nm.

With changing the thickness of graded layers, the rate of change of the relative refractive index changes and wave impedance of the graded layer also differ. The

modified wave impedance of the graded layers affects the intensity of the defect modes effectively. On the other hand, the effective refractive index changes are caused by the change of the layer thickness and hence, there is a change in the optical path length. The change makes a shift of the position of the defect modes. As is evidence from the results shown in figure 2.13, the generation of defect modes affected by the thickness of defect layer. Single defect mode observes in forbidden band gap of the structures of the form $(AB)^5ADA(BA)^5$ for the defect layer thickness equal to thickness of layer B and d/2, and defect mode absence in such structure for the defect layer thickness equal to 2d, and two defect mode form in the forbidden band gap of the structures with the defect layer thickness equal to 4d, as shown in the panels (a), (b), (c) and (d) of the figure 2.13, respectively. Accordingly, the generation of defect modes, defect mode frequency, and normalized mode intensity can be changed with the defect layer thickness.

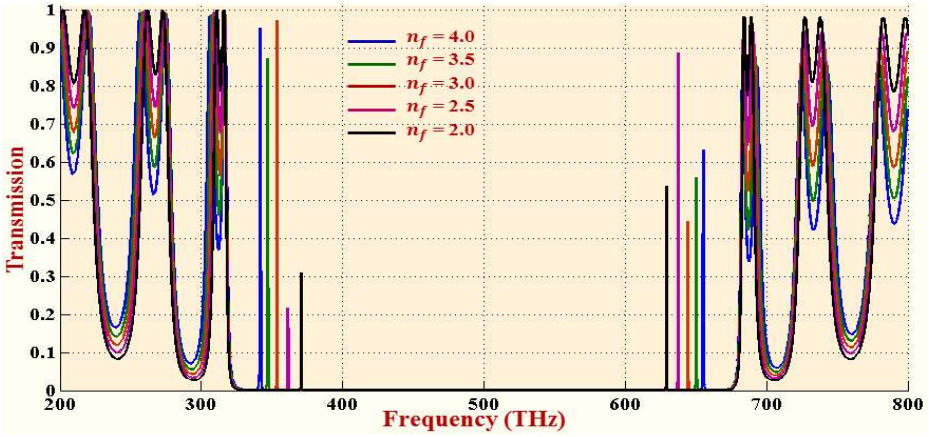

Figure 2.14 Transmission spectra at different values of contrast between initial ($\boldsymbol{n_i}$) and final ($\boldsymbol{n_f}$) refractive index of the graded index defect layer of the structure $(AB)^6ADA(BA)^6$. Refractive index $\boldsymbol{n_i = 1.5}$ and values of $\boldsymbol{n_f}$ are shown in the figure.

Likewise, the effect gradation parameters on the photonic defect modes for the quarter-wave stacked structures $(AB)^6ADA(BA)^6$ is shown in the figure 2.14. Here, we have considered the initial refractive index (n_i) of the graded index defect layer is fixed and equal to 1.5, while final refractive index (n_f) varies for different contrast values of n_i and n_f. As expected, defect modes frequency of both first and second defect modes are shifted toward central frequency and defect modes intensity change with changing the values of contrast of the initial and final refractive index of the graded layer, but forbidden band is unaffected by the contrast values. Due to decreasing the contrast values, the rate of change of the grading profile parameters (α) decreases and corresponding average refractive index of the volume of each graded layer also

decrease, hence influence of the Bragg stack to become less efficiently. Hence, the frequency and intensity of the defect modes can also be tuned by adjusting the grading profile parameters.

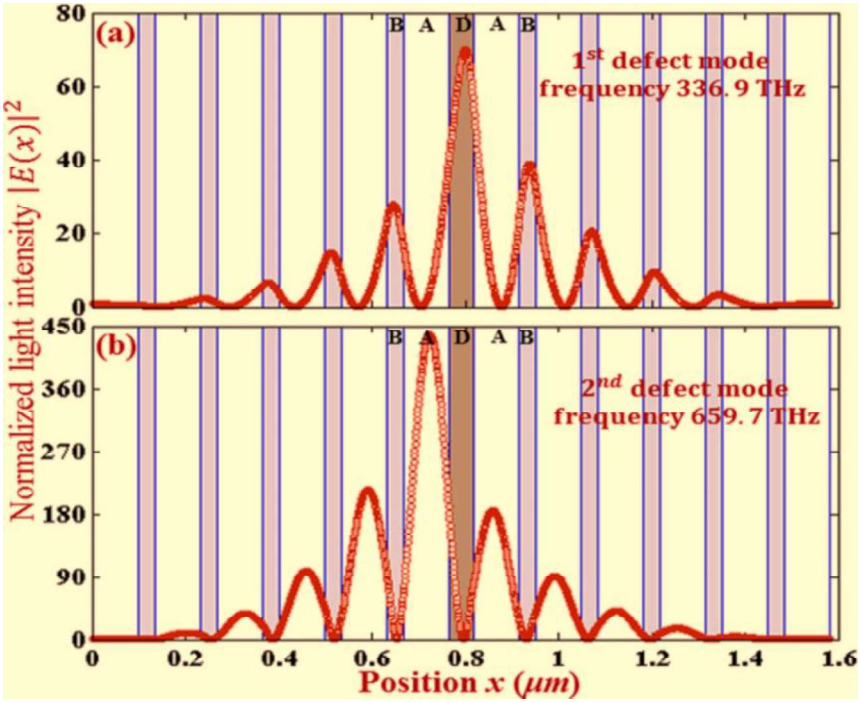

Figure 2.15 The electric field distribution at the defect modes frequency (a) 336.9 THz and (b) 659.7 THz in the defect structure form of $(AB)^5ADA(BA)^5$ containing defect layer as D of a linear graded index material.

In the conventional PCs, it is acknowledged that a defect mode is generally localized because of strong field localization within the defect at the corresponding defect mode frequency. It is accredited the diverse potential applications in the fields of optical devices based on field localizations [Liu (2014)]. Due to importance of the field localization, we have focused our study on the field distribution inside the structures with linear graded index material as a defect layer. The numerical simulations of the field distributions of the structure $(AB)^5ADA(BA)^5$ are shown in the figure 2.15. The strong localizations are obtained in the defect layer at the frequency of defect modes, and defect modes frequencies are 336.9 THz and 659.7 THz as can obtain from the transmittance spectra of the structure $(AB)^5ADA(BA)^5$. It can be seen that the electric field corresponding to first defect mode at frequency 336.9 THz is mainly localized in defect layer D shown in figure 2.15(a). On the other hand, the electric field corresponding to second defect mode at frequency 659.7 THz is mainly localized in central layer A as shown in figure 2.15(b). Therefore, the coupling layers A and D are

behaving two different kinds of effective defects and relate to the corresponding defect states at interface boundary of the graded index defect layer D. The characteristics of electric field distribution lead to the change of defect modes frequency and intensity.

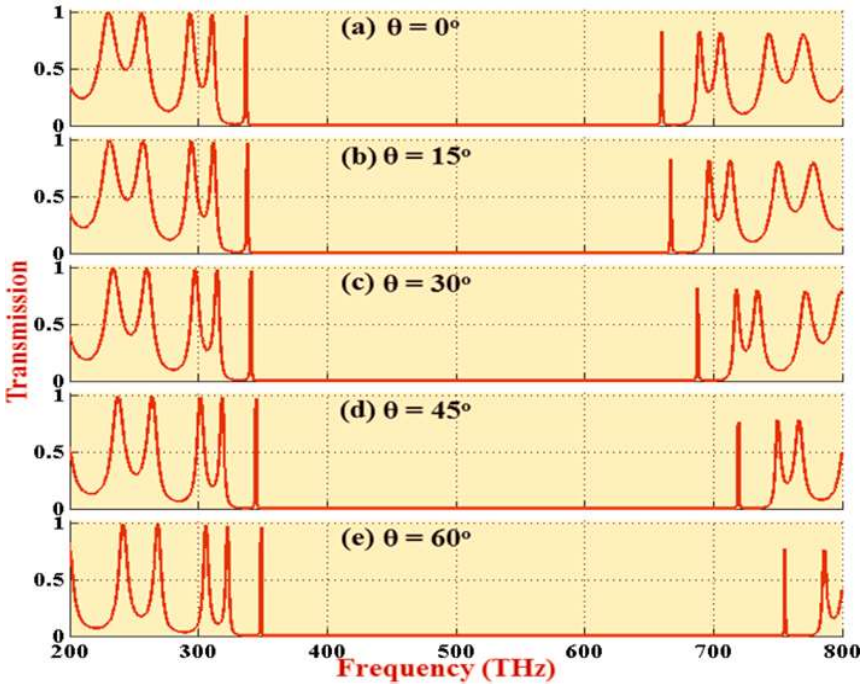

Figure 2.16 Transmission spectra at different incident angle (a) θ = 0°, (b) θ = 15°, (c) θ = 30°, (d) θ = 45° and (e) θ = 60° for TE-wave of the structure $(AB)^6ADA(BA)^6$ containing linear graded index defect layer as D.

Now, the influences of incident angle on the defect modes for TE and TM-polarization in the structure $(AB)^6ADA(BA)^6$ have investigated. The dependence of transmittance on the incident angle for TE-mode and TM-mode is shown in figure 2.16(a - e) and 2.17(a - e) corresponding to the incident angles from 0° to 60° with an interval of 15°. According to the transmission spectra, the defect modes frequency and intensity are change with the incident angle for both TE and TM-wave. It can also be seen that the defect modes of the structures are shift toward higher frequency with increasing the incident angle for both TE and TM-wave. The photonic bands of TE-wave are spreading toward the higher frequency, while that is shrinking but shift toward the higher frequency for TM-wave, with increasing the angle of incidence. The defect mode intensities also change with the incident angle for both TE and TM-wave. In order to discuss the variation of defect mode frequency (f_D) for TE and TM-wave, we have plotted the shifting frequency of the defect modes as a function of incident angle in figure 2.18(a) and 2.18(b), respectively. The variation of the defect mode frequency of

the first and second defect modes for both TE and TM-modes as changing the incident angle can clearly inspect from these figures.

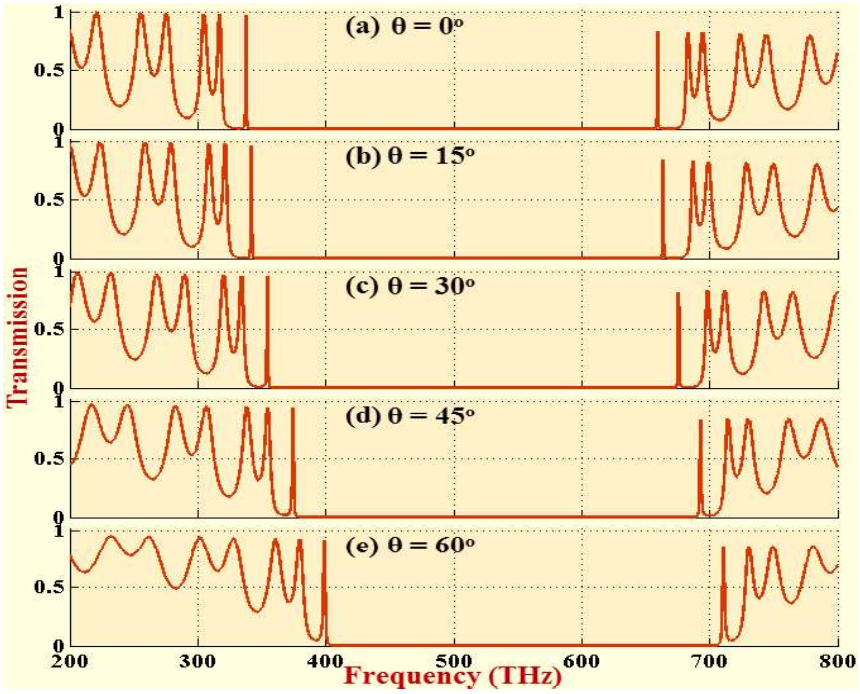

Figure 2.17 Transmission spectra at different incident angle (a) θ = 0°, (b) θ = 15°, (c) θ = 30°, (d) θ = 45° and (e) θ = 60° for TM-wave of the structure $(AB)^6ADA(BA)^6$ containing linear graded index defect layer as D.

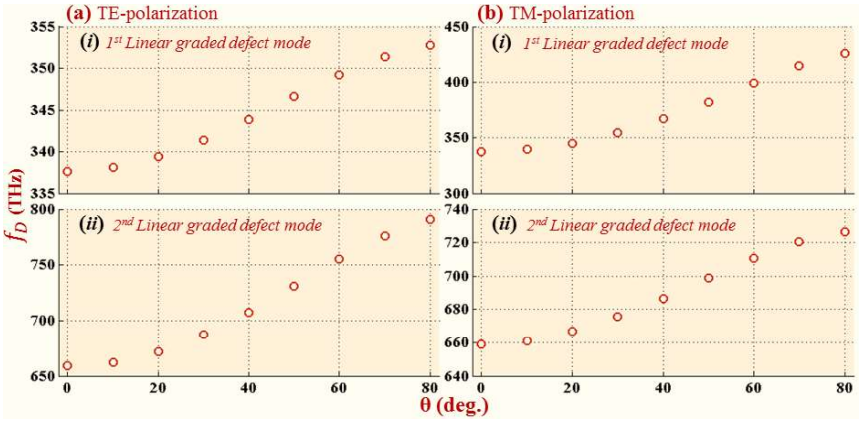

Figure 2.18 The dependence of defect mode frequency (f_D) on the incident angle (θ) for (a) TE-mode and (b) TM-mode in the structure form of $(AB)^6ADA(BA)^6$ containing linear graded index defect layer as D.

The defect modes frequency is shift toward the higher frequency with the incident angle. The variation of first defect mode frequency is very small in comparison to the second defect mode frequency for TE-wave while the changing of both defect mode frequencies is approximately same for TM-wave, with increasing the incident angle. In addition, the defect modes intensities for both TE-mode and TM-mode are also change

with the incident angle as depicted in figure 2.19(a) and 2.19(b), respectively. The intensities of both defect modes for TE-wave and TM-wave randomly change with the incident angle. Thus, the frequency position and intensity of the defect modes can also modulate by changing the incident angle and polarization.

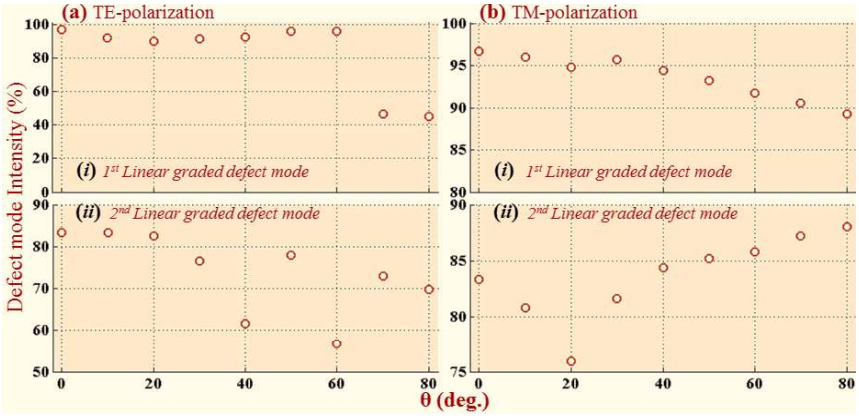

Figure 2.19 The dependence of defect mode intensity on the incident angle (θ) for (a) TE-mode and (b) TM-mode in the structure form of $(AB)^6ADA(BA)^6$ containing exponential graded index defect layer as D.

Accordingly, the average refractive index of the defect layer and different grading profile parameters have significant influence on the defect modes and their frequency position, intensity and electric field distribution in the structures. Hence, our investigations clearly demonstrate that the several structural parameters are accessible to tune the desirable defect modes in the 1-D PCs with linear graded index material as defect.

2.4 Conclusion

The influence of linear graded index materials on the photonic and omnidirectional band gap properties of 1-D periodic structures composed of linear graded and constant refractive index materials have been investigated. The number of photonic bands increases with layers thickness, while their bandwidths decrease as the increase of refractive index of the constituted homogeneous layer. The bandwidth of photonic bands also increases with the contrast of initial and final refractive index of the graded layers. The gradation profiles have a substantial influence on the reflection phase shift and electric field distribution in the structures. In addition, the omnidirectional band gap also exists when the relative refractive index of the homogeneous layer equal to 1.5 and 2.0, but it does not exist for 1.0. Thus, 1-D GPC structures with relative refractive index of the constituted homogeneous layer greater than 1.0 are suitable to

design the widespread omnidirectional band gap devices. For TE-polarization, 1-D GPC structures with the refractive index of the homogeneous layer equal to 1.0 have wide common reflection band. Therefore, these structures can be utilized especially for the configuration of TE-polarized devices. Thus, we can achieve the desired photonic and omnidirectional band gaps by selecting appropriate parameters of 1-D GPC structures.

Further, the tunability of photonic defect modes in 1-D PCs containing a defect layer of a gradual variation of refractive index in a linear fashion as a function of the depth of layer has investigated. The generation, position and intensity of defect modes can be modulated by changing with structural parameters, gradation profile, grading parameters, angle of incidence and polarization. The defect mode frequency and intensity of the defect modes also strongly depend on the contrast of initial and final refractive index of the constituted graded index defect layer, and the defect modes shift toward central frequency and their intensity also change with the values of contrast. In this way, the position and amplitude of the defect modes can control by adjusting the gradation profiles and parameters. We found the enhancement of electric field due to the localization of light in the defect layers. The defect mode frequencies and intensities of the defect modes can also be tuned by changing the incident angle and polarization. Thus, we expect to achieve desired defect modes by selecting appropriate structural and material parameters, gradation profiles, angles of incidence and polarizations in 1-D PC structures with linear graded index material as the defect.

These considered structures may be used to design various photonic devices such as mirrors, multi-channel filters, reflectors and optical sensors, etc. This work further opens the idea of understanding the effect of graded index materials and attaining the desired photonic and omnidirectional band gaps and defect modes in 1-D graded photonic crystals.

★★★★★★